Supporting Information

Three-dimensional Co_3O_4@C@Ni_3S_2 Sandwich-Structured Nanoneedle Arrays: Towards High-Performance Flexible All-Solid-State Asymmetric Supercapacitors

Dezhi Kong,[ab] Chuanwei Cheng,*[a] Ye Wang,[b] Jen It Wong,[b] Yaping Yang[a] and Hui Ying Yang*[b]

[a]*Shanghai Key Laboratory of Special Artificial Microstructure Materials and Technology, School of Physics Science and Engineering, Tongji University, Shanghai 200092, P.R. China,*

[b]*Pillar of Engineering Product Development, Singapore University of Technology and Design, 8 Somapah Road, Singapore 487372*

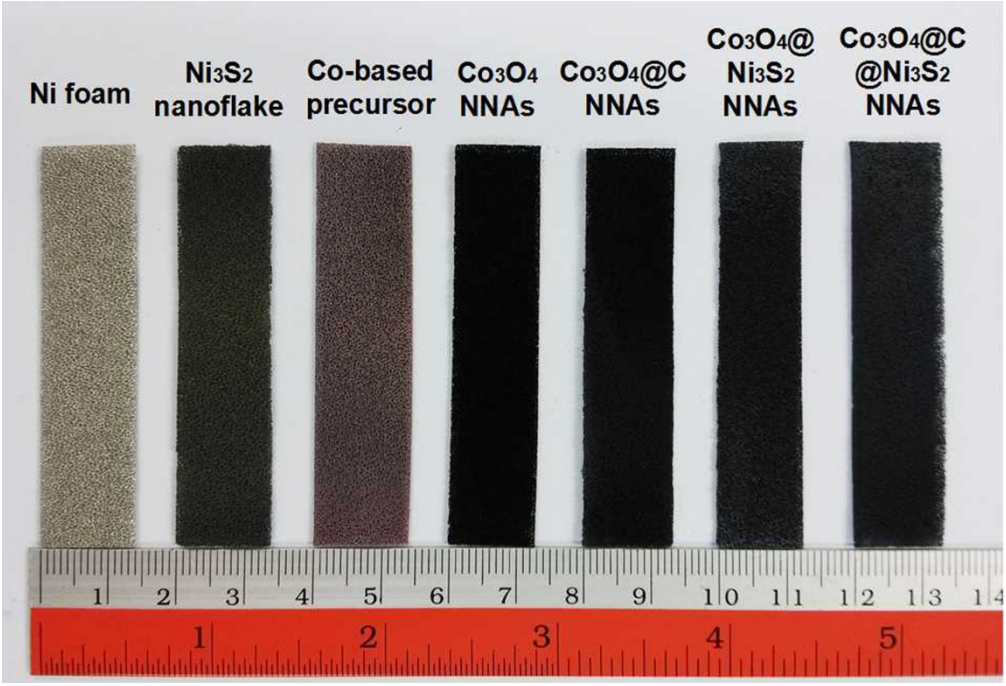

Figure S1 Photographs of nickel foam substrate, Ni_3S_2 nanoflakes on Ni foam, Co-based precursor on nickel foam, Co_3O_4 NNAs on Ni foam, Co_3O_4@C NNAs on Ni foam, Co_3O_4@Ni_3S_2 NNAs on Ni foam and Co_3O_4@C@Ni_3S_2 NNAs on Ni foam.

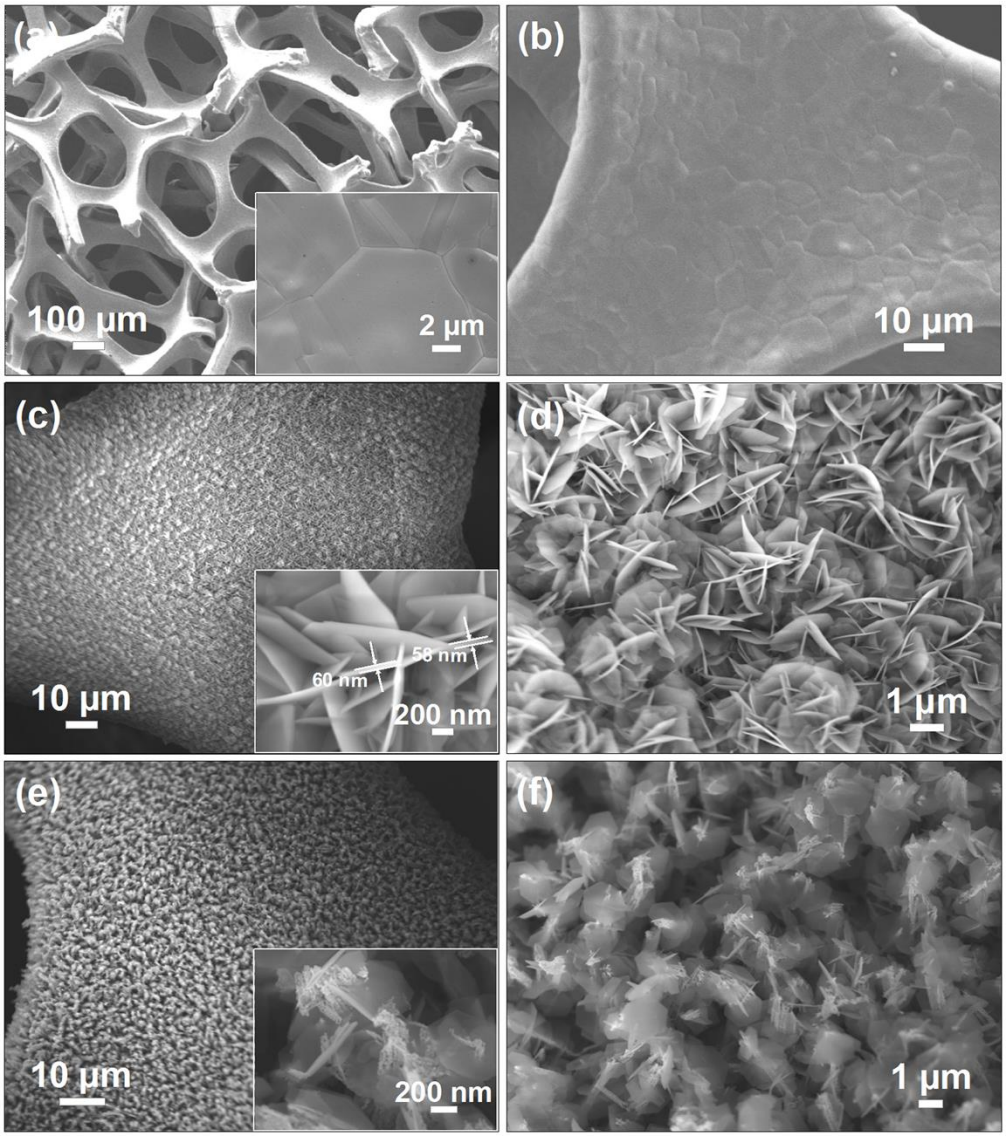

Figure S2 SEM micrographs of (a, b) pure Ni foam, (c, d) Ni_3S_2 nanoflakes and (e, f) Co_3O_4@Ni_3S_2 nanoneedle arrays on Ni foam.

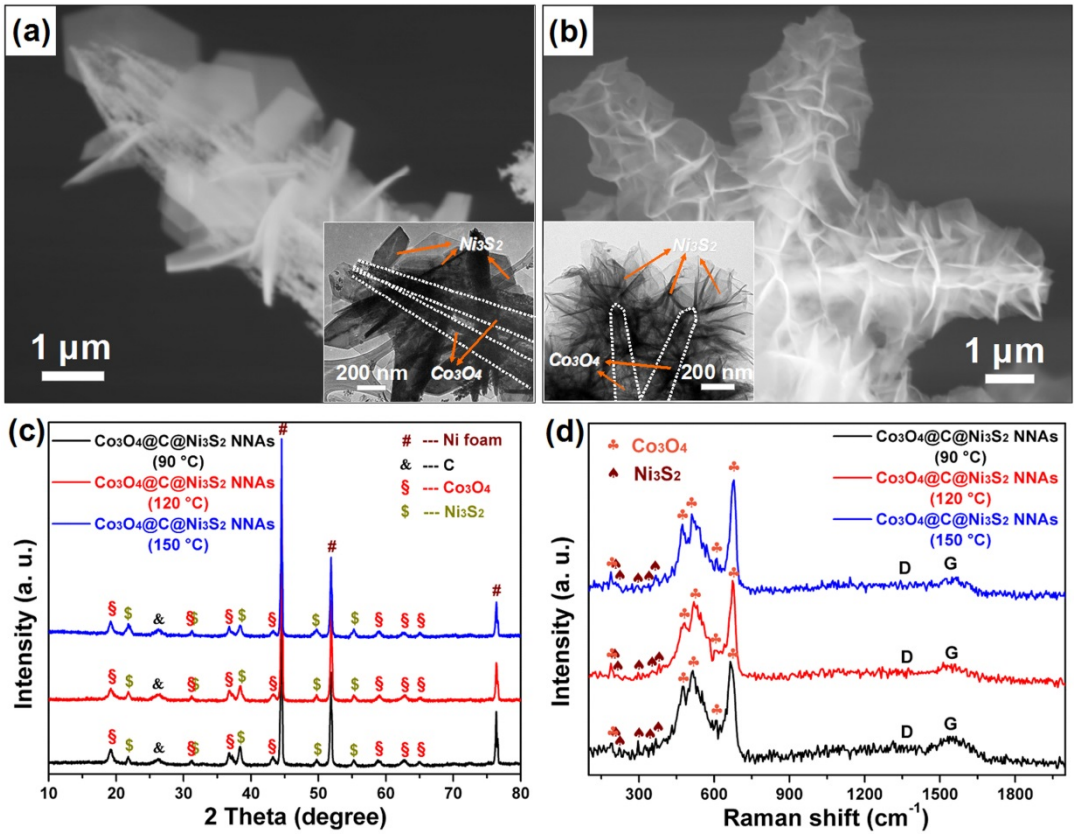

Figure S3 (a) SEM images of the Co_3O_4@C@Ni_3S_2 NNAs obtained at 90 °C of growth, and TEM image of a Co_3O_4@C@Ni_3S_2 NNAs was shown in the insets of (a); (b) SEM images of the Co_3O_4@C@Ni_3S_2 NNAs obtained at 150 °C of growth, and TEM image of a Co_3O_4@C @Ni_3S_2 NNAs was shown in the insets of (b); (c) XRD patterns and (d) Raman spectra of the Co_3O_4@C@Ni_3S_2 NNAs obtained with the same reaction stages except that different reaction temperatures in the second hydrothermal synthesis process: 90 °C, 120 °C and 150 °C.

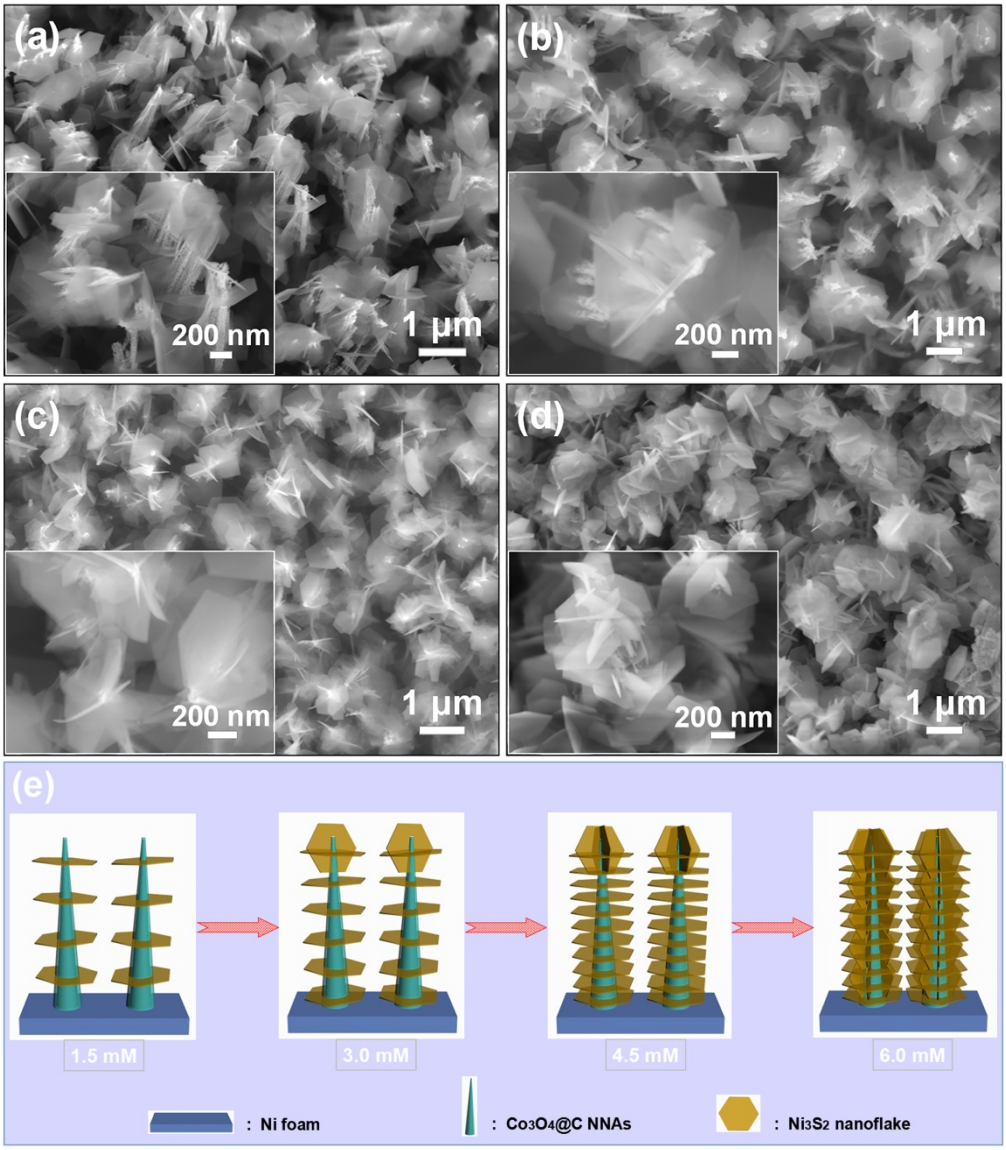

Figure S4 SEM images of the Co_3O_4@@C@Ni_3S_2 NNAs obtained with the same reaction stages except that different concentrations of aqueous mix solution ($Ni(NO_3)_2$ and thiourea) immersed in the second hydrothermal synthesis process: (a) 1.5 mM, (b) 3.0 mM, (c) 4.5 mM, (d) 6.0 mM; (e) Proposed mechanism for the effect of aqueous mix solution ($Ni(NO_3)_2$ and thiourea) on morphology construction.

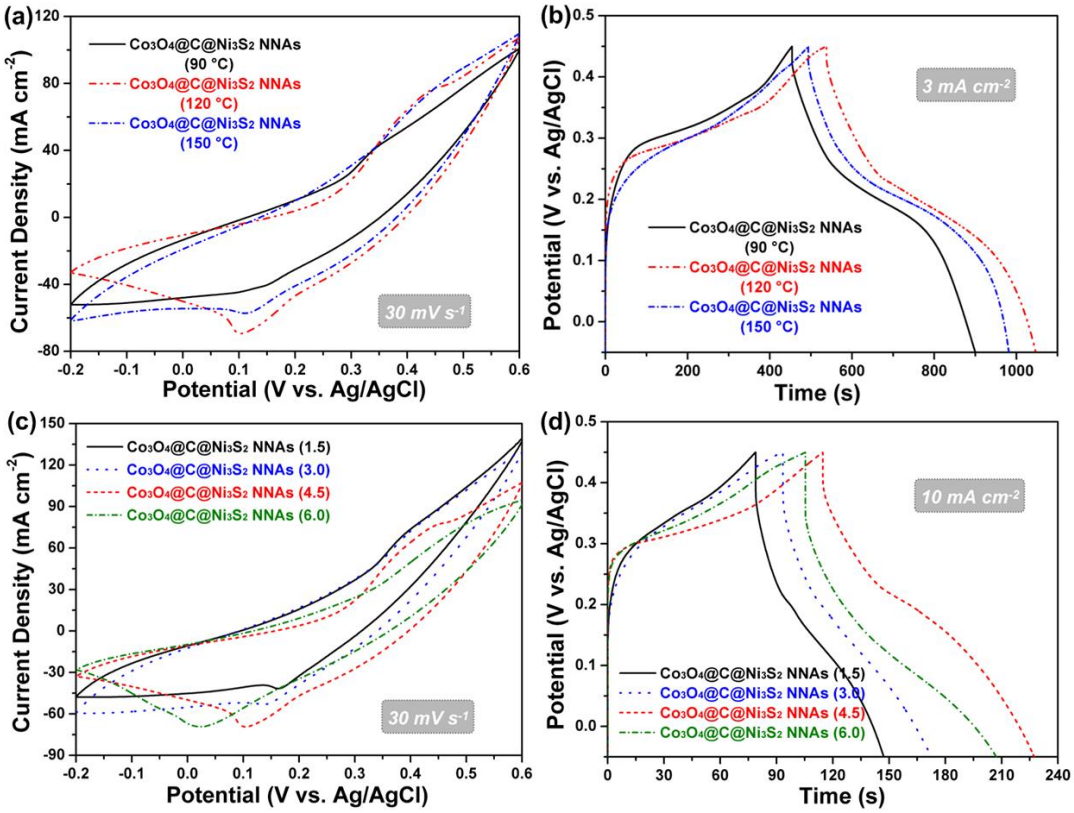

Figure S5 (a) CV and (b) galvanostatic charge-discharge curves of the Co_3O_4@C@Ni_3S_2 nanostructure arrays prepared different reaction temperatures in the second hydrothermal synthesis process, e. g. 90 °C (black curve), 120 °C (blue curve) and 150 °C (red curve); (c) CV and (d) galvanostatic charge-discharge curves of the Co_3O_4@C@Ni_3S_2 nanostructure arrays prepared various concentrations (e. g. 1.5 mM, 3.0 mM, 4.5 mM and 6.0 mM) of AMS at 120 °C in the second hydrothermal synthesis process.

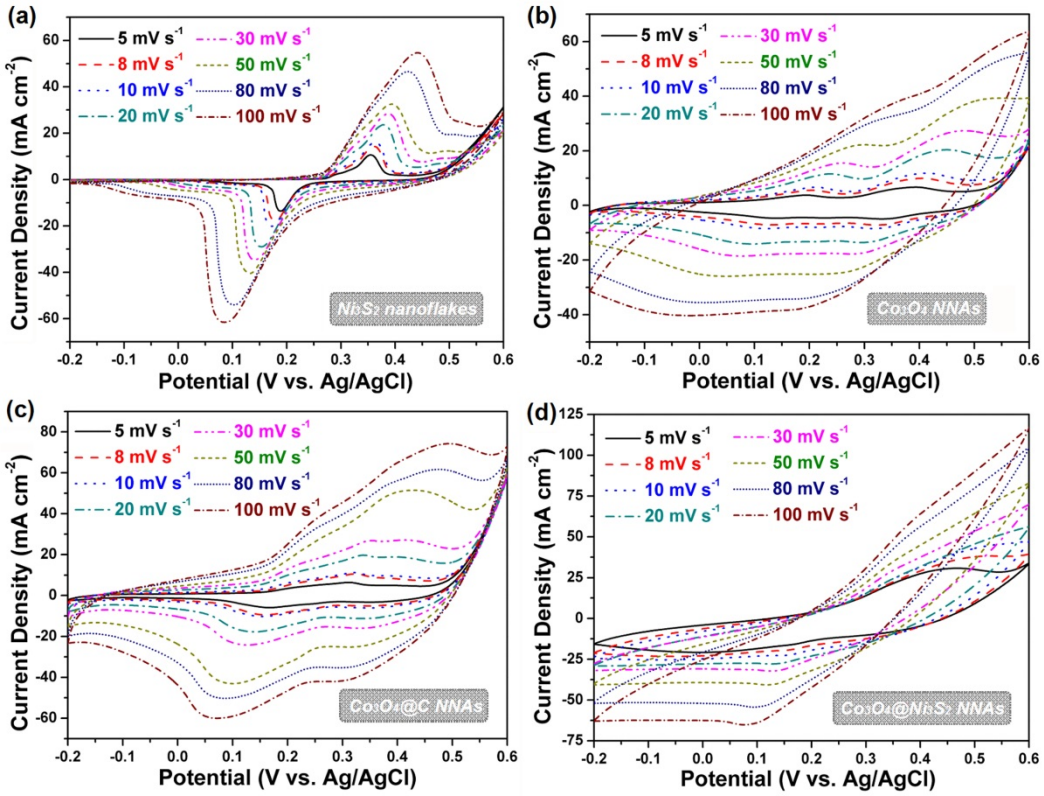

Figure S6 CV curves at different scan rates ranging from 5 to 100 mV s^{-1} of (a) the pure Ni_3S_2 nanoflakes, (b) bare Co_3O_4 nanoneedle arrays, (c) carbon-coating Co_3O_4 core-shell nanoneedle arrays, and (d) heterogeneous Co_3O_4@Ni_3S_2 core-shell nanoneedle arrays.

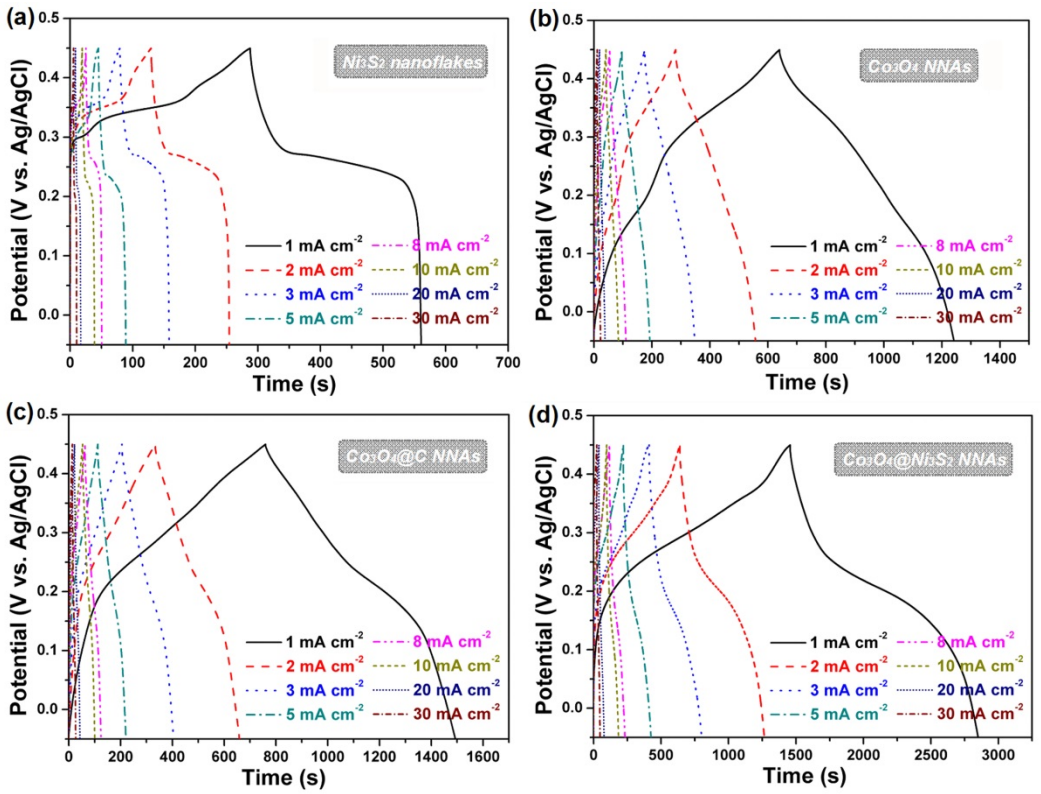

Figure S7 Galvanostatic charge-discharge curves at different scan rates ranging from 1 to 30 mA cm^{-2} of the (a) pure Ni_3S_2 nanoflakes, (b) bare Co_3O_4 nanoneedle arrays, (c) carbon-coating Co_3O_4 core-shell nanoneedle arrays, and (d) heterogeneous Co_3O_4@Ni_3S_2 core-shell nanoneedle arrays.

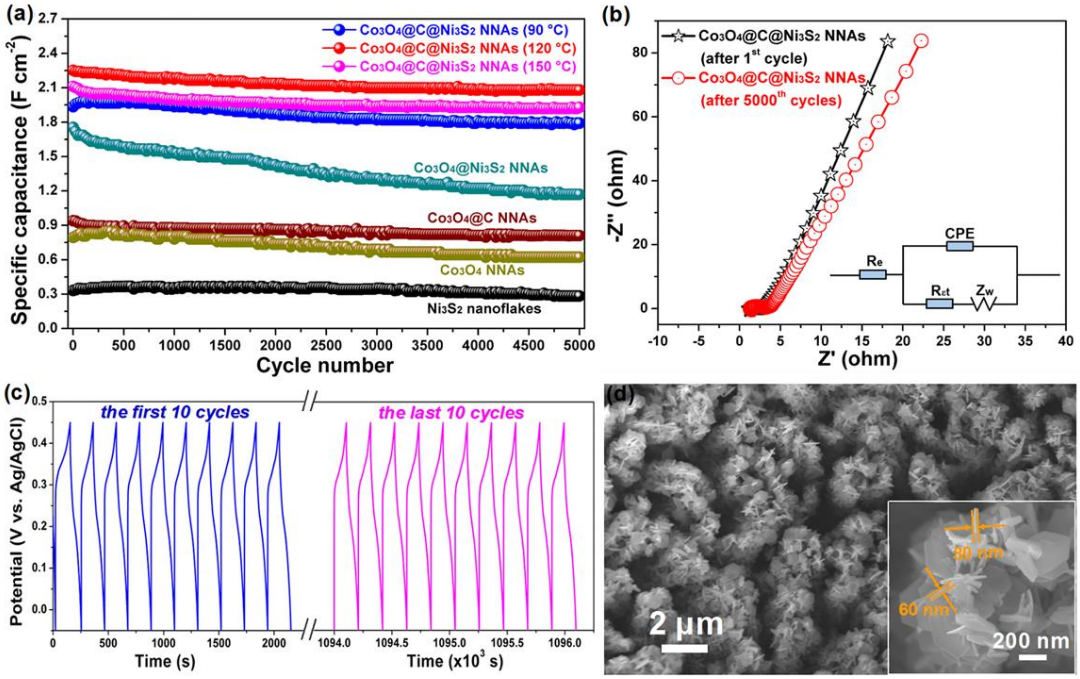

Figure S8 (a) Cycling performance of the Co_3O_4@C@Ni_3S_2 nanostructure arrays electrodes prepared at different reaction temperatures in the second hydrothermal synthesis process (5000 cycles), compared to Ni_3S_2 nanoflakes, Co_3O_4@NNAs, Co_3O_4@C NNAs and Co_3O_4@Ni_3S_2 NNAs electrodes; (b) Equivalent circuit and electrochemical impedance spectra of the Co_3O_4@C@Ni_3S_2 NNAs prepared at 120 °C after the first and 5000th cycles; (c) Charge-discharge curves of the first and the last 10 cycles at 10 mA cm^{-2} during 5000 cycles for the Co_3O_4@@C@Ni_3S_2 NNAs synthesized at 120 °C hydrothermal reaction, respectively; (d) Typical SEM image of the Co_3O_4@C@Ni_3S_2 NNAs prepared at 120 °C after 5000 cycles.

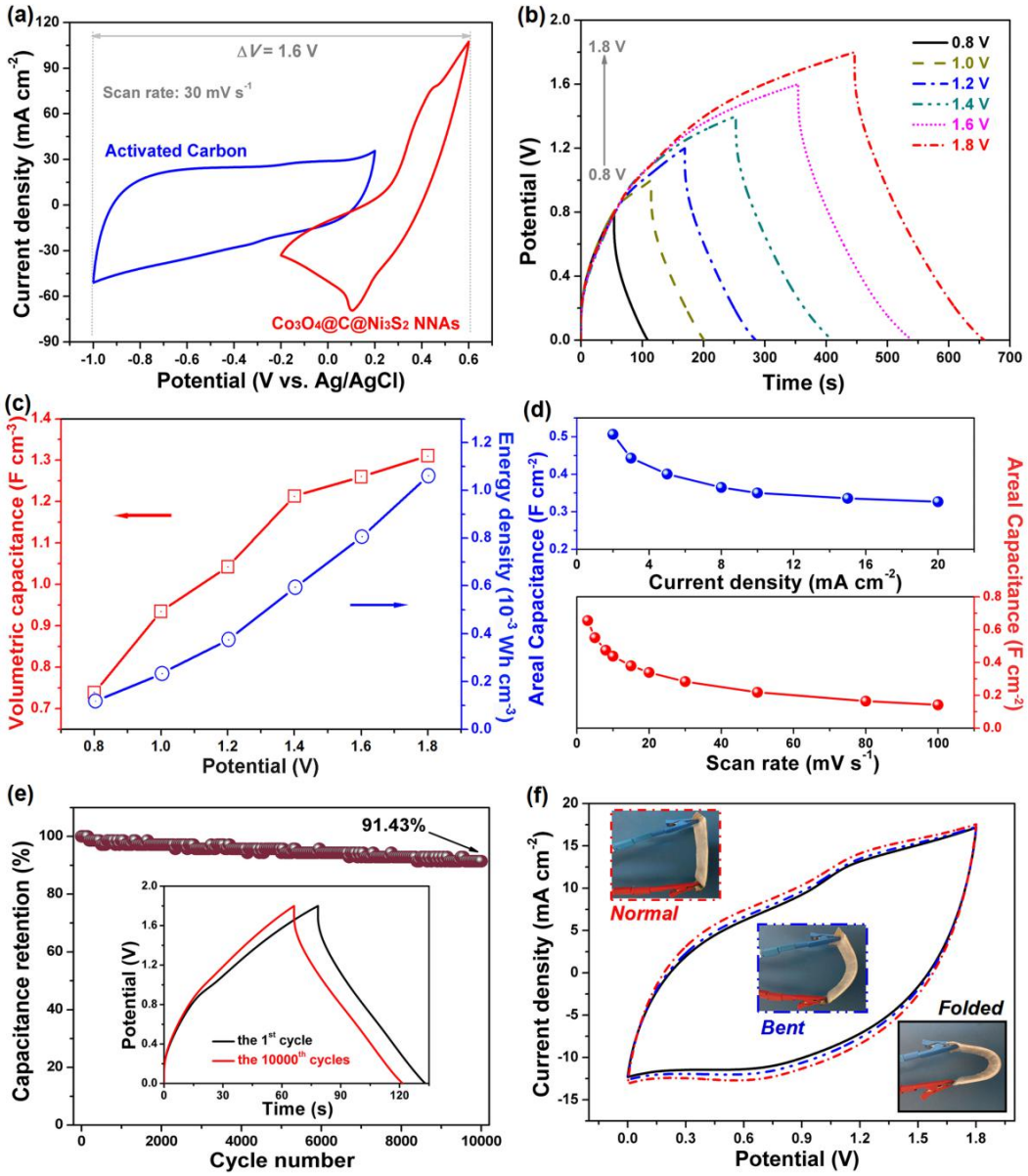

Figure S9 (a) The comparison of CV curves of the Co_3O_4@C@Ni_3S_2 NNAs composite and the activated carbon electrodes in -0.2 to 0.6 V and -1.0 to 0.2 V potential windows at a scan rate of 30 mV s^{-1}; (b) Galvanostatic discharge-charge curves collected at different potential windows for the Co_3O_4@C@Ni_3S_2//AC ASC device (3 mA cm^{-2}); (c) Volumetric capacitance calculated from CV and discharge curves as a function of potential window for the Co_3O_4@C@Ni_3S_2//AC ASC device; (d) Areal capacitance and capacitance retention of Co_3O_4@C@Ni_3S_2//AC ASC device calculated from the CV curves as a function of scan rate and the galvanostatic charge-discharge curves as a function of current density, respectively; (e) Cycling performance of ASC devices collected at a scan rate of 10 mA cm^{-2} for 10000 cycles in gel (KOH/PVA) electrolyte, and the inset is charge-discharge curves of the 1st and 10000th cycles for our device; (f) CV curves collected at a scan rate of 30 mV s^{-1} for the Co_3O_4@C@Ni_3S_2//AC ASC device under normal, bent, and folded conditions, and insets are the device pictures under test conditions.

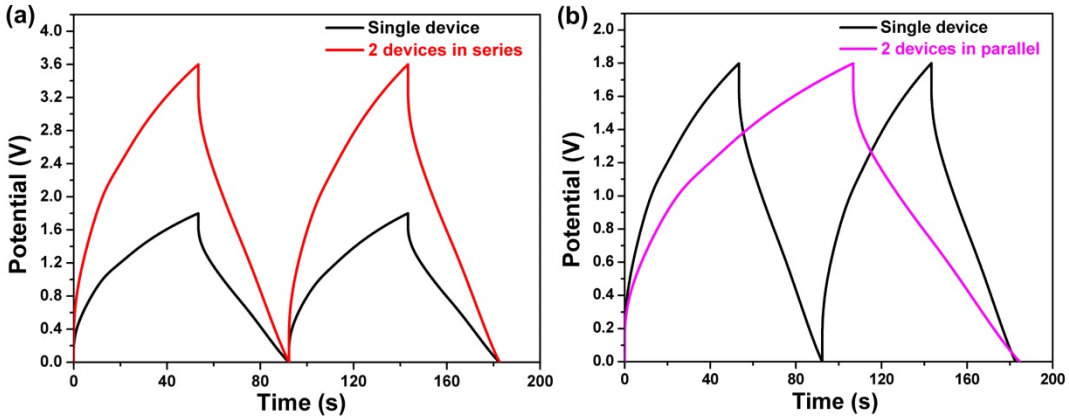

Figure S10 Galvanostatic charge-discharge curves at 10 mA cm^{-2} of a single solid-state supercapacitor (black curve) and two supercapacitors in (a) series (red curve) and (b) parallel (pink curve).